Dating the palaeolithic footprints of 'Le Rozel' (Normandy, France)

Norbert Mercier, Loïc Martin, Sebastian Kreutzer, Virginie Moineau, Dominique Cliquet

Dating the Palaeolithic Footprints of 'Le Rozel' (Normandy, France)

Norbert Mercier[1], Loïc Martin[1], Sebastian Kreutzer[1], Virginie Moineau[1], Dominique Cliquet[2]

1 - Institut de Recherche sur les Archéomatériaux, UMR 5060 CNRS - Université de Bordeaux Montaigne, Centre de Recherche en Physique Appliquée à l'Archéologie (CRP2A), Maison de l'archéologie, 33607 PESSAC Cedex, France.
2- Service Régional de l'Archéologie de Normandie, CAEN & UMR 6566 CNRS - Université de Rennes I, RENNES, France.

Corresponding author: Norbert Mercier (norbert.mercier@u-bordeaux-montaigne.fr)

Keywords: OSL dating, Le Rozel, Neandertal, footprints

Abstract
Luminescence ages were obtained from six sediment samples at the archaeological site 'Le Rozel'. These samples are associated with hundreds of footprints left by humans (probably Neanderthals) in the archaeological layers. The single-grain technique was applied to 200–250 µm quartz grains, whereas K-feldspar grains were measured using the multi-grain $pIRIR_{225}$ signal. For quartz, final D_e estimates were derived in applying a Bayesian model. The comparison of these minerals indicates that the K-feldspar ages are significantly higher than the quartz ages. Nevertheless, the OSL quartz measurements are in agreement with the sedimentological data, and consistent with previous OSL ages obtained in the 2000s for layers in a stratigraphical lower position. It was then concluded that feldspar grains have been likely insufficiently bleached due to the short transportation distance and/or because of a rapid burial by more recent sediments. Such a rapid sedimentation rate would also explain the good preservation of the found numerous human prints. Our new findings indicate that the site was inhabited during the outgoing MIS 5 and the footprints revealed an age of at least 70 ± 10 ka.

1. Introduction

The archaeological site of 'Le Rozel', located on the western part of the Cotentin peninsula (Normandy, France; Fig. 1) exhibits a long series of Mousterian occupations from the Upper Pleistocene period. The site was discovered in the 1960s and its importance immediately recognised (Scuvée, 1967, 1969). However, detailed investigations were not undertaken before the 1980s (Scuvée and Vérague, 1984). They revealed that the site preserved a long stratigraphic sequence which constitutes a valuable archive for reconstructing Upper Pleistocene environments in this part of Europe (Van Vliet-Lanoë et al., 2006). For that reason, in 2000, a series of sediment samples originating from the lower part of the stratigraphic sequence had been dated using multi-grain aliquots of quartz (Folz, 2000). These first results indicated that the lower part of the sequence covers the Marine Isotope Stage (MIS) 5 (Folz, 2000; Fig. 1).
In 2012, another large excavation under the supervision of D. Cliquet discovered numerous footprints in association with flint artefacts and fossilised remains of animals (Cliquet, 2016).

Such artefacts are typical for the Middle Palaeolithic period and believed having been produced by Neanderthals since, during this period, modern humans (i.e. *Homo sapiens*) were not supposed to live in Western Europe. Within five succeeding field seasons, a total number of 450 prints (including handprints) had been identified and studied. Today the site constitutes the largest known series of palaeolithic human prints (Cliquet, 2016). The importance of this discovery led to a new dating study focused on the archaeological layers containing the prints, for which the results are presented here. Conversely to the previous OSL study, the single-grain technique has been applied to quartz grains, and comparisons with K-feldspars ages were systematically undertaken for the sediments sampled.

2. Site stratigraphy and samples location

Figure 2 shows a synthetic profile revealing the stratigraphic sequence. At the base, the sequence (Unit D1) is composed of large rounded pebbles which are interpreted as the beach remnants formed during MIS 5e (Van Vliet-Lanoë et al., 2006). The upper part of unit D1 as well as the overlying units D2 and D3 are composed of sands or silt sediments. These units are interpreted as indicators of past climatic variations characterising the transitions from MIS 5d to MIS 5a (ca. 109–82 ka; cf. MIS scale by Lisiecki and Raymo, 2005). Intercalated small solifluction layers (D3a1-D3c) have been identified in Unit D3 which also contains several archaeological layers rich in lithic artefacts, animal bones and footprints. To account for its archaeological relevance, our dating study focused on this unit (D3). In total six sediment samples were taken within this unit. All our samples (black dots on Fig. 2) are located in a stratigraphical higher position than the samples OSL-dated in 2000 (open dots on Fig. 2: Folz, 2000), and should thus be younger.

3. Sample preparation and dosimetry

3.1 Sample preparation

Samples were prepared under orange, subdued, light conditions. The sediment was split into two parts: 100 g were kept for high resolution gamma-ray spectrometry analysis while the other fraction was prepared using conventional sample preparation methods for luminescence dating (e.g., Preusser et al., 2008). Granulometric analyses of our samples done with sieves suggested a great homogeneity of all samples (their massic fractions were very similar: ca. 5 % for <200 µm; ca. 20% for 200–250 µm and ca. 75% for >250 µm); thus, they all consisted mainly of fine and medium sand. The 200–250 µm fraction was finally chosen for the sample preparation. After sieving, this fraction was treated with HCl (10%), then H_2O_2 (30%) and a part of it was then treated with HF (40%, 40 min) to dissolve feldspar grains and then rinsed in HCl (10%) and demineralised water. The etched fraction was later used for OSL quartz. The other part was kept untreated and later used for IRSL measurements on feldspar grains. For this series of analyses, feldspar grains were extracted from the untreated HF fraction using heavy liquids at a density of 2.56 g/cm^3.

3.2 Field dosimetry

On site, in situ gamma-ray measurements were performed. Therefore, a LaBr gamma probe (connected to a Canberra Inspector 1000 electronic handheld), calibrated using the threshold technique (Mercier and Falguères, 2007) was used. The holes left in the profile by the sampling have been used after they have been slightly enlarged to allow the insertion of the probe. The

measured gamma dose-rates are given in Table 1, and range from 226–364 µGy/a. The cosmic dose-rate was not measured on site but estimated according to the depth of the sample position (Prescott and Hutton, 1994); its value was estimated to 150±30 µGy/a.

3.3 Laboratory dosimetry

High resolution low-level gamma-ray spectrometry was performed on the preserved fractions after the sediments were dried and stored in sealed plastic boxes for at least three weeks. U, Th, K contents were found to be similar for all samples (Table 1), ranging from 0.39–0.48 ppm for U, from 1.02–1.61 ppm for Th, and from 0.66–0.83 % for K. No radioactive disequilibria were detected in the U-series chain. The measured water contents ranged from 8–12% and a mean value of 10% was taken for the dose rate calculation. The gamma dose-rates determined from the U, Th, K contents give values close to those measured on site with the LaBr probe, indicating that the sediments are homogeneous in terms of radioelements distribution at a scale of at least ten of centimetres.

The U, Th, K data also allowed to compute the infinite matrix beta dose-rate of each sample (Table 1) using the dose rate conversion factors by Guérin et al. (2011), and the attenuation factors by Guérin et al., 2012. However, such calculation assumes that all radioelements are homogeneously distributed in the sediment at a scale much lower than the range of the particles depositing the dose, i.e. here 2–3 mm for beta-particles. This assumption is only partly true for our samples. The sediments contain feldspar grains which may have a high K-content, acting as hot-spots, especially if their proportion in mass is low (Guérin et al. 2012). Moreover, the granulometric distribution of our sediments which is characterised by a large fraction above 250 µm, may also affect the beta dose rate received by the grains used for the D_e estimation. To tackle these impacts, grains from sample S1-2 (from the fraction untreated with HF) were analysed with scanning electron microscopy (SEM): the proportion of K-feldspar grains was determined and their internal K-content measured. An averaged K-content of 10±2% was obtained for the investigated grains. To better assess the impact of these feldspathic grains on the beta dose rate, in a second step a model of the sediment was created with the software *DosiVox* (Martin et al., 2015a). The model considers the granulometric distribution of the sample, the proportion of feldspar grains as well as their mean K-content. The numerical simulation by *DosiVox* indicates that quartz grains with a grain size of 200 µm have been exposed to a beta dose-rate (due to the found K content), which is on average ca. 7% higher than the value computed by the infinite matrix assumption. Nevertheless, taking into account the contribution of U and Th to the total beta dose rate received by these quartz grains, the resulting total beta dose rate represents already 59% of the total dose rate (including gamma and cosmic doses). Thus, we deduced that the difference in dose rates between the infinite matrix model (in which the radioelements are homogeneously distributed, exactly as they would be if the sediment were a liquid) and a model in which the feldspar grains (rich in K in comparison to the sediment) are explicitly represented, does not exceed 4%. However, the simulation also shows that a small proportion of grains received a beta dose rate much higher (almost two times higher) than the mean value (a similar result had already been obtained by Martin et al. (2015b) for a series of sediment samples). The heterogeneity in the beta dose rates received by the 200 µm grains may then contribute significantly to the over-dispersion characterising the D_e distribution of this sample. Nevertheless, this conclusion is not necessarily valid for to other samples. The result depends on the proportion of feldspathic grains and on the granulometric distribution and, is thus sample dependent.

4. Luminescence measurements

4.1 Equipment

Both multi-grains and single-grain luminescence analyses were performed. All multi-grain measurements were carried out on a Freiberg Instruments *lexsyg SMART* reader (Richter et al., 2015). The reader was equipped with an Hamamatsu H7360-02 photomultiplier tube and a Sr-90/Y-90 β-source delivering ca. 11 Gy/min to 90–180 µm quartz grains (Risø calibration quartz, batches 90 and 106). For quartz, green LEDs (525 Δ 25 nm) delivering a maximum power density of 70 mW/cm^2 were used and the luminescence signal in the UV was detected through a Schott BG-3 (3 mm) in conjunction with a Chroma BP365/50 EX interference filter. Feldspars were measured on the same machine using IR stimulation (850 Δ 3 nm, max. 300 mW/cm^2) and the signal was detected in the blue-violet range through a Schott BG-39 (3 mm) in combination with an AHF BrightLine HC 414/46 interference filter.
For quartz single-grain measurements, a Risø TL/OSL DA-20 reader (Bøtter-Jensen et al., 2000; 2003) was used. This device was equipped for stimulation with a 10 mW Nd:YVO_4 solid-state diode-pumped laser emitting at 532 nm (max. 103 mW/cm^2). The signal was detected through a 7.5 mm Hoya U-340 filter in front of an EMI 9235QB15 photomultiplier tube. The inbuilt Sr-90/Y-90 β-source allowed irradiations with a dose rate of ca. 8.3 Gy/min to 200–250µm quartz grains.

4.2 Quartz measurements

Preliminary tests were carried out on multi-grain aliquots. It was first checked that the quartz extracts (200–250µm fractions) did not give significant signals when stimulated with IR (measured IR/OSL ratio lower than 2%). Moreover, comparisons of the OSL signals from our samples and from the Risø calibration quartz indicated that the fast component was dominant. Dose recovery tests (DRT) were then performed using different preheat temperatures on a series of aliquots of sample S3. Artificial bleaching was carried out with a Hönle Sol500 solar simulator. For measurements, a single-aliquot and regenerative dose (SAR) protocol (Murray and Wintle, 2000; 2003) was used. The measurement sequence included a systematic measure of thermal transfer, recycling ratio and a IR depletion test included at the single grain level (Duller, 2003). The data were analysed with Analyst (Duller 2015; v4.31).

The DRT results are shown on Fig. 3 indicating no trend with increasing temperature, but a plateau over the investigated temperature range. Finally, a preheat temperature of 260°C for 10 s, and a cutheat temperature of 160°C for 0 s were chosen for subsequent measurements. Before determining single-grain equivalent dose (D_e) values, a second dose recovery test was performed on 1,200 single-grains of sample S3: 105 out of 1,200 grains (i.e. ~8.7%) passed the chosen selection criteria (thermal transfer < 5%; recycling ratio < 10%; maximum test dose error = 20%). The recovered to given dose ratio was 0.99±0.05, justifying the application of this protocol (preheat treatment at 260°C for 10 s for natural and regenerated signals, cutheat at 160°C for test dose signals). For this DRT test, the over-dispersion (OD) was 14±2 % if a common dose is assumed. For determining individual D_e values, 12 single-grain discs of each sample were measured and signals evaluated using the criteria previously determined with the DRT. Additionally, grains giving a natural signal close to or even higher than the maximum regenerated signal were also discarded. Depending on the sample, only between 46 to 55

grains were selected and the Central Age Model (CAM: Galbraith et al., 1999) used for calculating D_e values (Table 2). As indicated in the same table, OD values range from 29 (sample S3) to 47% (sample S1-2) but the Abanico plots (Dietze et al., 2016) do not show any trend which might indicate poor bleaching of the selected quartz grains, whatever is the OD value (Fig. 4). To support this observation, the Finite Mixture Model was applied to samples S1-2 and S3 using the function *calc_FiniteMixture* (Burow, 2017), with a sigma-b value of 0.14 (similar to the OD value determined with the DRT test). The results indicate that the De distributions are best represented by 2 components with one component gathering together 69% (sample S1-2) and 70% (sample S3) of the population. But for sample S1-2, the main component is the first one, while for sample S3, it is the second. This seems indicate that partial bleaching is not the source of scatter of the individual De values.

The study by Guérin et al. (2015) suggested that the CAM under-estimates the mean D_e and also returns a D_e-error which is not comparable to the error associated with the dose rate value (Guérin et al., 2013). These authors estimated that the difference between the CAM and the Bayesian model ('baSAR') by Combès et al. (2015), which is supposed to overcome the inherent problems affecting the CAM and assumes a Cauchy distribution of the individual D_e values instead of a log-normal distribution for the CAM, was significant in the temporal range of 4–46 ka. For the samples from Le Rozel, we then computed D_e values with the baSAR model, in using the **R** (R Core Team, 2017) function `analyse_baSAR()` proposed by Mercier et al. (2016) and available in the 'Luminescence' package (Kreutzer et al., 2012; Kreutzer et al., 2017). To compute the central dose (cf. Combès et al., 2015; Mercier et al., 2016), we applied a single saturating exponential dose response curve and did not include the recycling points in the calculation. Similar conditions were chosen for D_e values which had been used for calculating the CAM. In the temporal range covers by our study (between 70 ka to 90 ka), the comparison of the two sets of results indicates that the baSAR D_e values are between 4 % to 17% higher than the CAM D_e values (Table 2). Since the baSAR model has been shown to be less sensitive to outliers than the CAM (Guérin et al. (2015), we preferred the D_e values derived from the baSAR model and their associated uncertainties to compute the quartz OSL ages given in Table 2.

4.3 Feldspars measurements

Since feldspar grains were also present in our sediment samples, we tested the post IR IRSL approach by Thomsen et al., 2008. Post-IR IRSL (henceforth pIRIR) signals were measured with IR stimulation temperatures of 50°C and 225°C ($pIRIR_{225}$). The protocol followed the suggestions by Buylaert et al., 2009. After measurement of any natural of regenerative signal, a test dose of 15 Gy was given for normalisation. All preheats were carried out at 250°C for 60s (natural, regenerated and test dose signals). Measurements were done with multi-grains aliquots of 5 mm in diameter and performed in nitrogen atmosphere.

4.3.1 Feldspars – tests

The bleachability of the $pIRIR_{225}$ signal was evaluated by exposing aliquots of sample S3 (natural dose ca. 200 Gy) to our solar simulator for durations of {0, 1, 5, 22,48} h. This device provides an intensity of ~800 W/m^2 which is six times higher than the natural sunlight. In our case, after 22 hours, the natural dose had been reduced by 98.5%. The residual dose was estimated to ca. 2 Gy (Fig. 5). After 48 hours, the dose reduction reached >99%. These results indicate that the $pIRIR_{225}$ signal can be well bleached by solar light exposure, but these

experiments do not inform on potential residual doses at the time of deposition. Consequently, we did not subtract any residual dose when calculating ages from the pIRIR data.
Fading tests were performed with the same sample. Five aliquots were bleached for 48 hours with the solar simulator, before being irradiated with 150 Gy. Prompt preheat and measurements following Auclair et al. (2003) were applied. The $pIRIR_{225}$ signals were measured after different delays (0, 24, 300 h). The fading rate, normalized to 2 days (g_{2d}) was 2.36±0.6 %. The large relative uncertainty (~25%) reflects the apparent different behaviours of the aliquots. Fig. 6 shows for 4 out of 5 aliquots a significant decrease of the normalised $pIRIR_{225}$ signal if one compares the 24h and 300h points to the 0h point, but a similar decrease (expected on a logarithm scale) is not visible between the 24h and 300h points. The reason of this behaviour was not further investigated but might be related to a not corrected sensitivity change or another process as a short-term fading. Only for one aliquot the normalised signals followed a logarithmic scale as expected.

4.3.2 Feldspars – Dose recovery test and equivalent doses

A dose recovery test was done with five aliquots of sample S3 bleached for 48 h with the solar simulator and irradiated with 183 Gy. A SAR pIRIR protocol similar to Buylaert et al. (2009) was used for estimating the D_e. The sequence was composed of seven cycles with regenerative doses of {45, 153, 275, 450, 0, 45} Gy and, as for the previous tests performed with feldspars, used a test dose of 15 Gy and all preheats were set at 250°C for 60s. The dose recovery test ratio was close to unity (0.96±0.05) indicating that this protocol allows recovering a known dose similar in size to the expected naturally absorbed dose. For each sample, this protocol was applied to a series of 20 aliquots (except sample S3 for which 26 aliquots were measured). Fig. 7 shows a typical dose-response curve of the normalised $pIRIR_{225}$ signal. For the six samples, the mean D_e values are similar, ranging from ~143 Gy to ~152 Gy (Table 2).
Table 2 also contains mean D_e values calculated after the dose rate correction (DRC) method (Lamothe et al., 2003) has been applied to individual aliquots, considering the measured fading rate (g_{2d}=2.36±0.6). Fading-corrected mean D_e values are given in Table 2 and are on average 36% higher than the uncorrected values. This large difference is caused mainly by the fading rate which leads to a significant increase of the Ln/Tn ratio, and to a less extent by the curvature of the growth curve.

5. Ages calculation and discussion

Ages were calculated both for quartz and feldspars data (Table 2).
For quartz, ages range from 70 ± 10 ka to 86 ± 9 ka (MIS 4 to MIS 5c) but do not exactly follow the stratigraphic order. However, considering the associated errors, they are all indistinguishable. This relatively low scatter was expected since all samples have been taken in a unit with a presumably high sedimentation rate, otherwise, the footprints would have not been preserved. These new OSL ages closely associated with the footprints are younger than the results obtained in 2000 for sediment samples taken lower in the stratigraphy (Fig. 2), and which gave ages concordant with MIS 5, as expected. Our data also indicate that large OD values do not necessarily characterise poorly bleached grains: for instance, sample S1-2 (OD value of 47±6%) gives an OSL age in good agreement with the other samples exhibiting lower OD values. We thus conclude that micro-dosimetric heterogeneities account for a part of the

observed OD values, as demonstrated by the numerical simulation using *DosiVox*, and that this particular contribution is sample dependent.
By contrast, the feldspar ages (Table 2) are older than the quartz ages, ranging from 114 ± 11 ka to 126 ± 12 ka, but five out of six of them are in the range 122 ± 12 ka to 126 ± 12 ka. These ages are likely over-estimated and consequently too old in comparison of the stratigraphical evidence, in particular, the presence of the Eemian deposit (MIS 5e) in unit D1. Two reasons may explain this over-estimation: (1) No residual dose was subtracted and even though the measured $pIRIR_{225}$ signal proved itself as well bleachable in the laboratory, it might be higher in nature (insufficient bleaching). (2) The fading correction used a rate which might not be representative of the true fading affecting our samples. More work (single grain measurements on feldspars, long-term fading measurements) will be necessary to explore these uncontrolled parameters.

6. Conclusion

New luminescence dating results were presented for the archaeological site 'Le Rozel'. We applied single-grain OSL on quartz separates and $pIRIR_{225}$ measurements on K-feldspar extracts. Despite the encountered inconsistencies between OSL quartz and $pIRIR_{225}$ ages, the OSL ages calculated in applying the baSAR model to individual single-grain data were found in agreement with the previously obtained dating results as well as with the sedimentological data. It believes that poor bleaching of K-feldspar grains and the use of an inappropriate fading rate may explain the large over-estimation of the pIRIR results. We also noticed that high OD values - up to 47% - obtained when measuring single-grains of quartz are not necessarily characterising poorly bleached samples, but may indicate dosimetric heterogeneities at the millimeter scale. Our OSL samples clearly indicate that unit D3 in which were discovered hundreds of human prints is characterised by a high sedimentation rate, what explains the good preservation of these numerous prints. Finally, one concludes that the Le Rozel site was occupied during the outgoing MIS 5 by a group of humans (probably Neanderthals) who left their prints in the archaeological layers.

Acknowledgments
The authors are grateful to the LaScArBx (ANR-10-LABX-52) for financial support.

References

Auclair, M., Lamothe, M., Huot, S., 2003. Measurement of anomalous fading for feldspar IRSL using SAR. Radiation Measurements 37, 487-492.

Bøtter-Jensen, L., Bulur, E., Duller, G.A.T., Murray, A.S., 2000. Advances in luminescence instrument systems. Radiation Measurements 32, 523-528.

Bøtter-Jensen, L., McKeever, S.W.S., Wintle, A., 2003. Optically Stimulated Luminescence Dosimetry. Elsevier, Amsterdam.

Burow, C. (2017). calc_FiniteMixture(): Apply the finite mixture model (FMM) after Galbraith (2005) to a given De distribution. Function version 0.4. In: Kreutzer, S., Dietze, M., Burow, C., Fuchs, M.C., Schmidt, C., Fischer, M., Friedrich, J. (2017). Luminescence: Comprehensive Luminescence Dating Data Analysis. R package version 0.7.5. https://CRAN.R-project.org/package=Luminescence

Buylaert, J.P., Murray, A.S., Thomsen, K.J., Jain, M., 2009. Testing the potential of an elevated temperature IRSL signal from K-feldspar. Radiation Measurements 44, 560-565.

Cliquet D., 2016. Néandertal au Rozel. Association historique de Surtainville. 3, 61 p.

Combès B, Lanos P, Philippe A, Mercier N, Tribolo C, Guérin G, Guibert P, Lahaye C (2015). Quaternary Geochronology 28: 62-70.

Dietze, M., Kreutzer, S., Burow, C., Fuchs, M.C., Fischer, M., Schmidt, C., 2016. The abanico plot: visualising chronometric data with individual standard errors. Quaternary Geochronology 31, 12–18. doi:10.1016/j.quageo.2015.09.003

Duller, G.A.T. 2003. Distinguishing quartz and feldspar in single grain luminescence measurements. Radiation Measurements 37, 161–5.

Duller, G.A.T., 2015. The Analyst software package for luminescence data: overview and recent improvements. Ancient TL 33, 35–42.

Folz E., 2000. La luminescence stimulée optiquement du quartz : développements méthodologiques et applications à la datation de séquences du Pléistocène supérieur du Nord-Ouest de la France. Thèse de doctorat, Université de Paris 7, 267 p.

Galbraith, R.F., Roberts, R.G., Laslett, G.M., Yoshida, H., Olley, J.M., 1999. Optical dating of single grains of quartz from Jinmium rock shelter, northern Australia. Part I: experimental design and statistical models. Archaeometry 41, 339-364.

Guérin, G., Mercier, N., Adamiec, G., 2011. Dose-rate conversion factors: update. Ancient TL 29 (1), 5-8.

Guérin, G., Mercier, N., Nathan, R., Adamiec, G., Lefrais, Y., 2012. On the use of the infinite matrix assumption and associated concepts: a critical review. Radiation Measurements 47, 778-785.

Guérin, G., Murray, A. S., Jain, M., Thomsen, K. J., Mercier, N., 2013. How confident are we in the chronology of the transition between Howieson's Poort and Still Bay? Journal of Human Evolution 64 (4), 314-316.

Guérin, G., Combès, B., Tribolo, C., Lahaye, C., Mercier, N. Guibert, P. Thomsen, K. J., 2015. Testing the accuracy of a single grain OSL Bayesian central dose model with known-age samples. Radiation Measurements 81, 62-70.

Kreutzer S, Schmidt C, Fuchs MC, Dietze M, Fischer M, Fuchs M (2012). Ancient TL 30: 1–8. Martin L, Mercier N, Incerti S., 2015. Ancient TL 33 (1), 1-10.

Kreutzer, S, Dietze, M, Burow, C, Fuchs, M C Fuchs, Schmidt, C, Fischer, M. Friedrich, J., 2017. Luminescence: Comprehensive Luminescence Dating Data Analysis. R package version 0.7.3. https://CRAN.R-project.org/package=Luminescence

Lamothe, M., Auclair, M., Hamzaoui, C., Huot, S., 2003. Towards a prediction of longterm anomalous fading of feldspar IRSL. Radiation Measurements 37, 493-498.

Lisiecki, L.E., Raymo, M.E., 2005. A Pliocene-Pleistocene stack of 57 globally distributed benthic δ ^{18}O records. Paleoceanography 20, 1–17. doi:10.1029/2004PA001071

Martin, L., Incerti, S. and Mercier, N., 2015a. DosiVox: Implementing Geant 4-based software for dosimetry simulations relevant to luminescence and ESR dating techniques. Ancient TL 33(1), 1-10.

Martin, L., Mercier, N., Incerti, S., Lefrais, Y., Pecheyran, C., Guérin, G., Jarry, M., Bruxelles, L., Bon, F., Pallier, C., 2015b. Dosimetric study of sediments at the Beta dose rate scale: characterization and modelization with the DosiVox software. Radiation Measurements 81, 134-141.

Mercier, N., Falguères, C., 2007. Field gamma dose-rate measurement with a NaI(Tl) detector: re-evaluation of the "threshold" technique. Ancient TL 25 (1), 1-4.

Mercier, N., Kreutzer, S., Christophe, C., Guérin, G., Guibert, P., Lahaye, C., Lanos, Ph., Philippe, A., Tribolo, C., 2016. Bayesian statistics analysis in the R Luminescence package : the analyse_baSAR function. Ancient TL 34 (2), 14-21.

Murray, A.S., Wintle, A.G., 2000. Luminescence dating of quartz using an improved single-aliquot regenerative-dose protocol. Radiation Measurements 32, 57-73.

Murray, A.S., Wintle, A.G., 2003. The single aliquot regenerative dose protocol: potential for improvements in reliability. Radiation Measurements 37, 377-381.

Prescott, J.R., Hutton, J.T., 1994. Cosmic ray contributions to dose rates for luminescence and ESR dating: large depths and long-term time variations. Radiation Measurements 23, 497-500.

Preusser, F., Degering, D., Fuchs, M., Hilgers, A., Kadereit, A., Klasen, N., Krbetschek, M.R., Richter, D., Spencer, J.Q.G., 2008. Luminescence dating: basics, methods and applications. Eiszeitalter und Gegenwart (Quaternary Science Journal) 57, 95–149.

R Core Team, 2017. R: A Language and Environment for Statistical Computing. R Foundation for Statistical Computing, Vienna, Austria.https://r-project.org

Richter, D., Richter, A., Dornich, K., 2015. Lexsyg smart — a luminescence detection system

for dosimetry, material research and dating application. Geochronometria 42, 202–209.

Scuvée F., 1967. Le Rozel : Trou du renard. Rapport de fouilles ronéoté, 10 p.

Scuvée F., 1969. Le Rozel : Trou du renard. Rapport de fouilles ronéoté, 12 p., 5 fig., 7 pl.

Scuvée F., Vérague J., 1984. Paléolithique supérieur en Normandie occidentale : l'abri-sous-roche de la pointe du Rozel (Manche). Cherbourg, LITTUS-C.E.H.P., 150 p.

Van Vliet-Lanoë B., Cliquet D., Auguste P., Folz E., Keen D., Schwenninger J.-L., Mercier N., Alix P., Roupin Y., Meurisse M. et Seignac H., 2006. L'abri sous-roche du Rozel (France, Manche): un habitat de la phase récente du Paléolithique moyen dans son contexte géomorphologique. Quaternaire 17 (3), 207-258.

Figure and table captions:

Figure 1: Location of the Le Rozel site in Normandy (France).

Figure 2: Stratigraphic profile of the Le Rozel sequence. Black dots indicate the location of the samples dated in this study. Open dots are sediment samples OSL-dated by Folz (2000).

Figure 3: Dose recovery tests results performed on multi-grains (quartz) aliquots of sample S3 for preheat temperatures of 200, 220, 240, 260 and 280°C (applied to regenerated doses). Cut heat was 160°C for 0 s (applied to test dose).

Figure 4: Abanico plots for samples S1-2 and S3. OD values are 47 % and 29 %, respectively, but no trend which might indicate poor bleaching of grains, is visible whatever is the OD.

Figure 5: Decrease of the residual dose in feldspar grains measured with the $pIRIR_{225}$ signal. Bleaching was with a Hönle SOL500 solar simulator.

Figure 6: Fading test results. The signal loss was measured using the prompt $pIRIR_{225}$ signal and delay times of 24 h and 300 h.

Figure 7: Dose response curve of the $pIRIR2_{225}$ signal as a function of dose. The open dot corresponds to the normalised natural signal after fading correction with the DRC method.

Table 1: Radioactive (U, Th, K) contents of the sediment samples deduced from spectrometric analyses. The annual dose rate includes a cosmic contribution of 150±30 µGy/a and the annual dose rate for feldspars includes an internal beta contribution assuming a K-content of 10±2% for feldspar grains. A water content of 10±2% was assumed for all samples.

Table 2: Equivalent doses, overdispersion (OD) and ages for the 6 samples of this study. All quartz results have been obtained in analysing single grains. The quartz OSL ages were obtained considering the baSAR D_e values. For feldspars, multi-grains analyses were done. A fading correction using the DRC method (Lamothe et al., 2003) was applied to the individual aliquots.

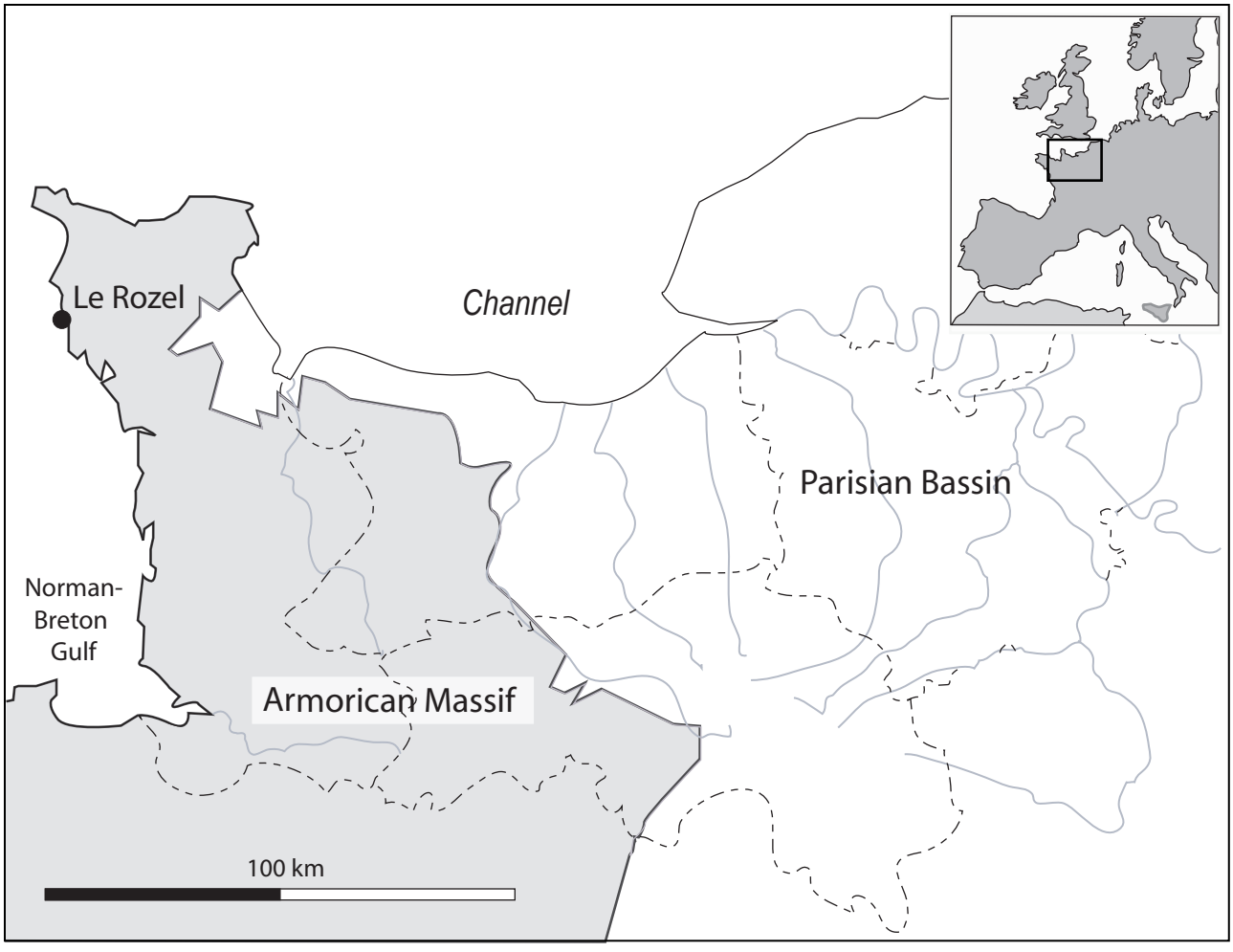
Le Rozel
Channel
Parisian Bassin
Norman-
Breton
Gulf
Armorican Massif
100 km

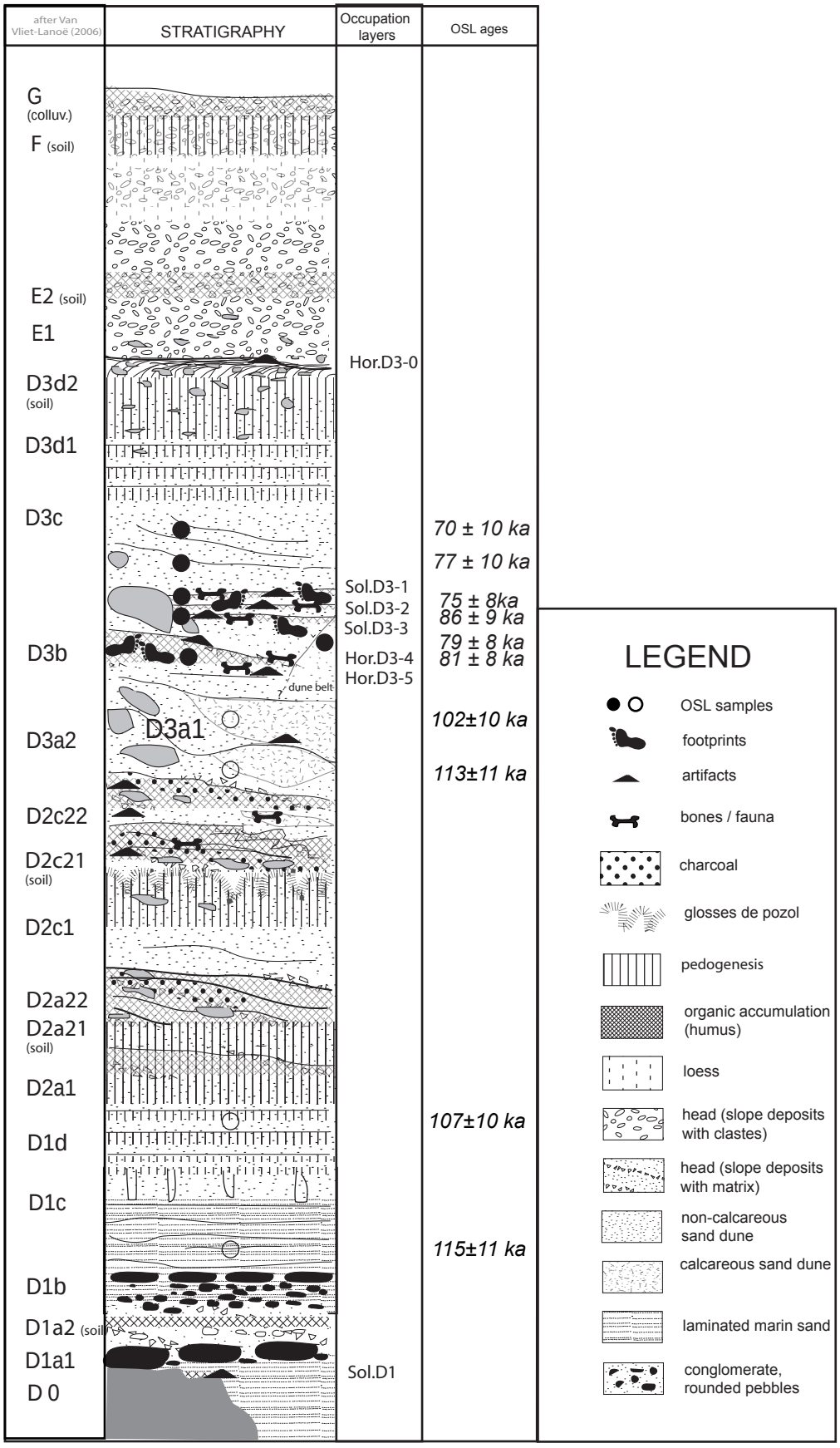
after Van Vliet-Lanoë (2006)
STRATIGRAPHY
Occupation layers
OSL ages
G (colluv.)
F (soil)
E2 (soil)
E1
D3d2 (soil)
D3d1
D3c
D3b
D3a2
D2c22
D2c21 (soil)
D2c1
D2a22
D2a21 (soil)
D2a1
D1d
D1c
D1b
D1a2 (soil)
D1a1
D 0
D3a1
dune belt
Hor.D3-0
Sol.D3-1
Sol.D3-2
Sol.D3-3
Hor.D3-4
Hor.D3-5
Sol.D1
70 ± 10 ka
77 ± 10 ka
75 ± 8ka
86 ± 9 ka
79 ± 8 ka
81 ± 8 ka
102±10 ka
113±11 ka
107±10 ka
115±11 ka
LEGEND
OSL samples
footprints
artifacts
bones / fauna
charcoal
glosses de pozol
pedogenesis
organic accumulation (humus)
loess
head (slope deposits with clastes)
head (slope deposits with matrix)
non-calcareous sand dune
calcareous sand dune
laminated marin sand
conglomerate, rounded pebbles

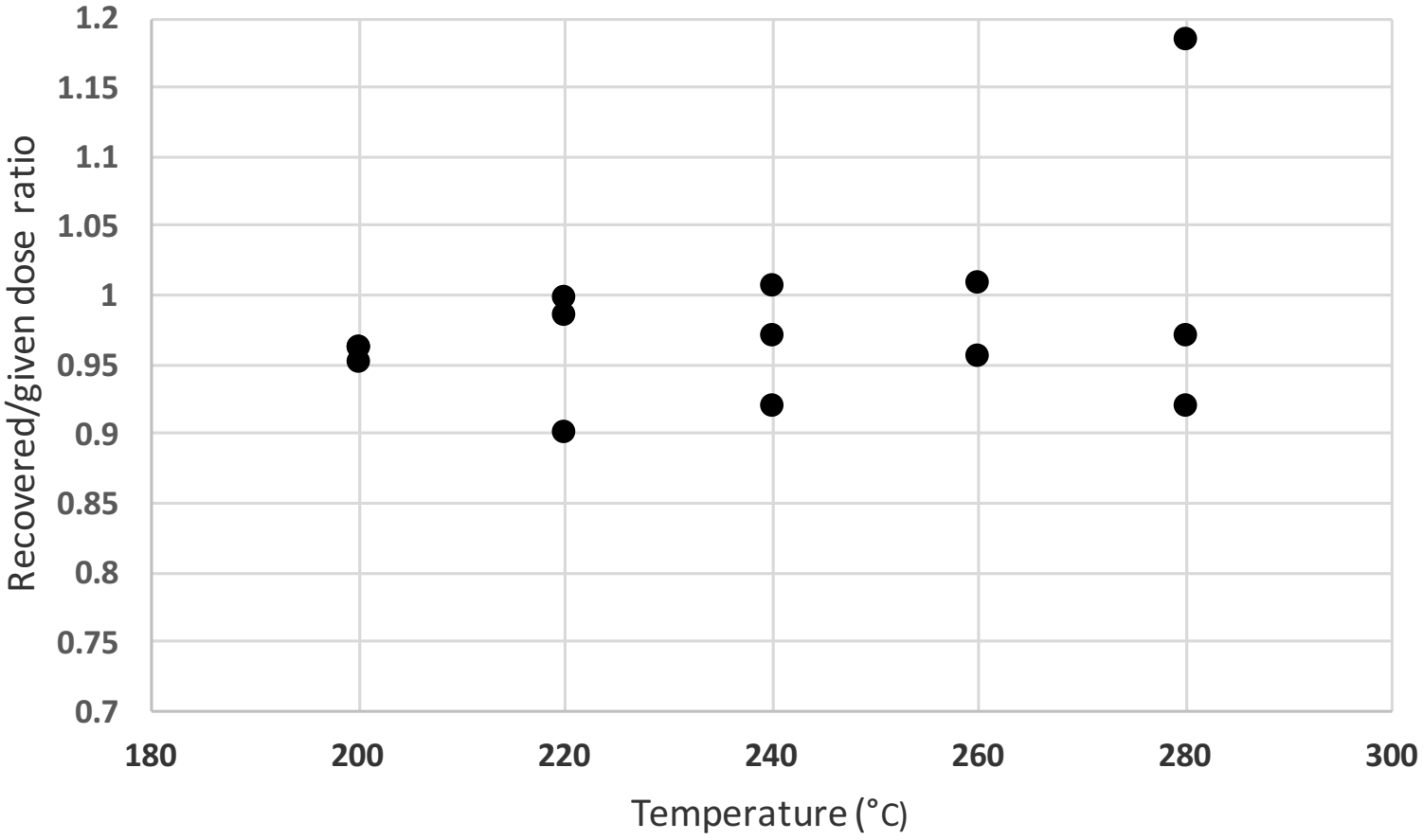
Recovered/given dose ratio
1.2
1.15
1.1
1.05
1
0.95
0.9
0.85
0.8
0.75
0.7
180
200
220
240
260
280
300
Temperature (°C)

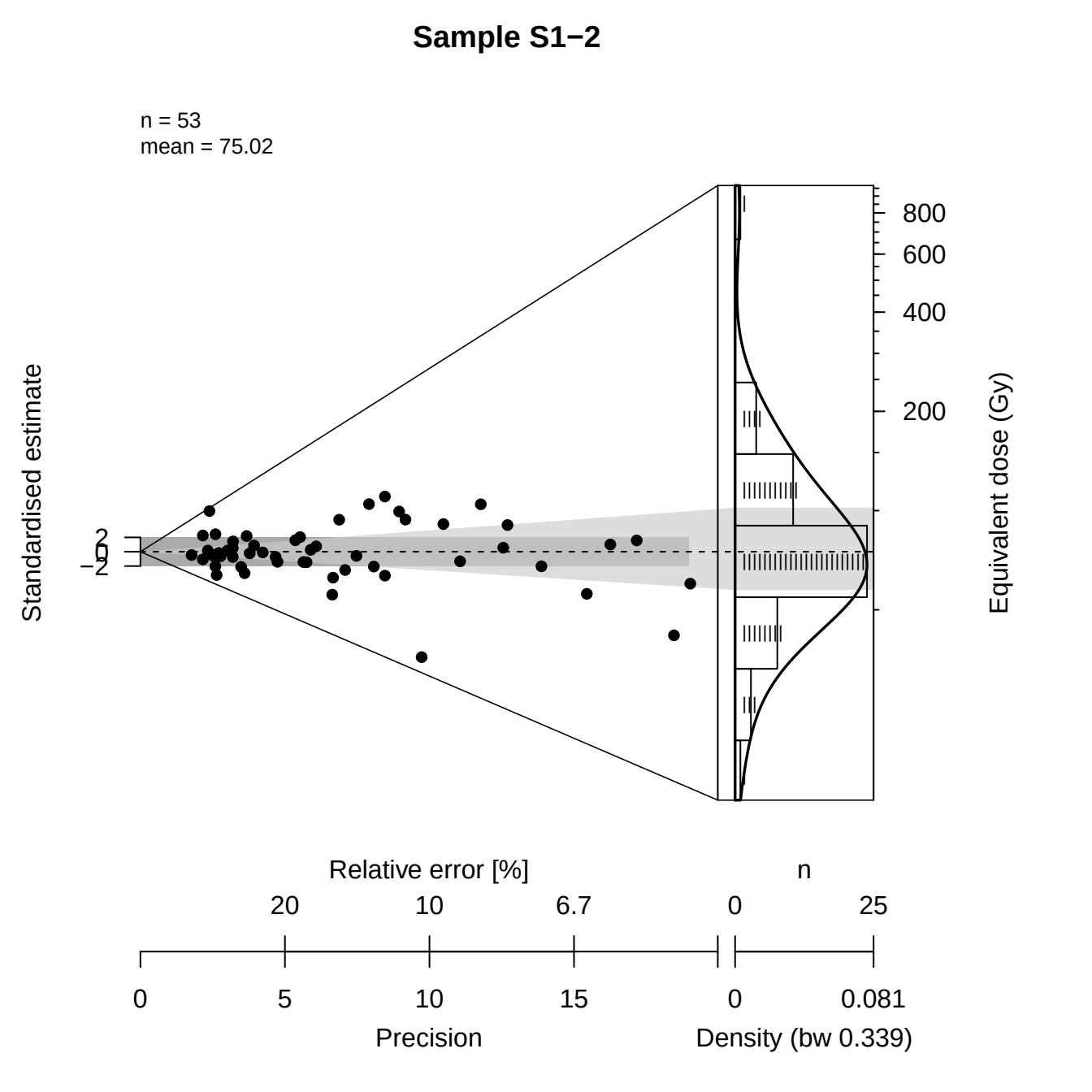
Sample S1−2
n = 53
mean = 75.02
Standardised estimate
2
0
−2
800
600
400
200
Equivalent dose (Gy)
Relative error [%]
20
10
6.7
0
n
25
0
5
10
15
Precision
0
0.081
Density (bw 0.339)

Sample S3

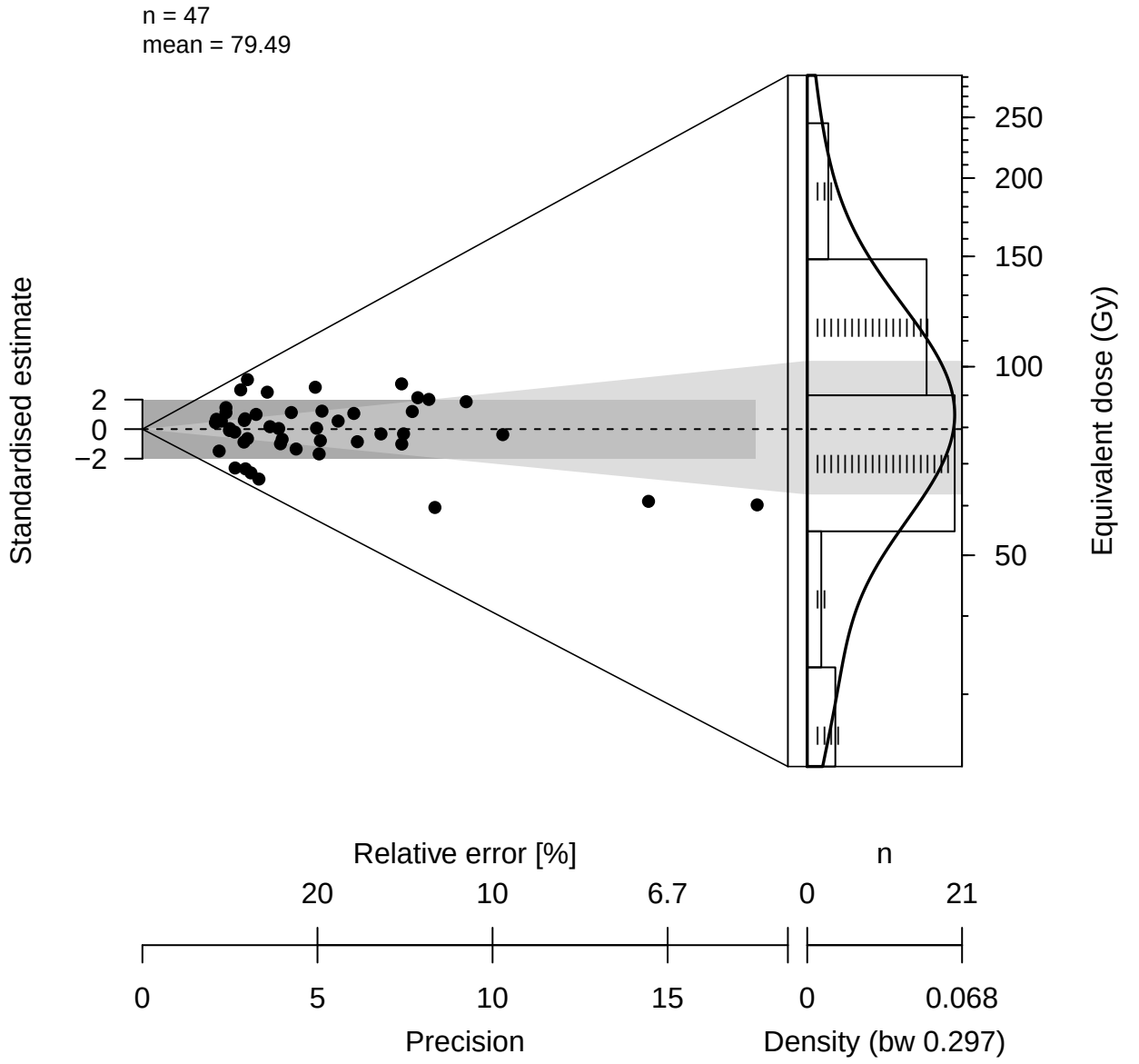
n = 47
mean = 79.49
Standardised estimate
2
0
−2
250
200
150
100
50
Equivalent dose (Gy)
Relative error [%]
20
10
6.7
0
n
21
0
5
10
15
0
0.068
Precision
Density (bw 0.297)

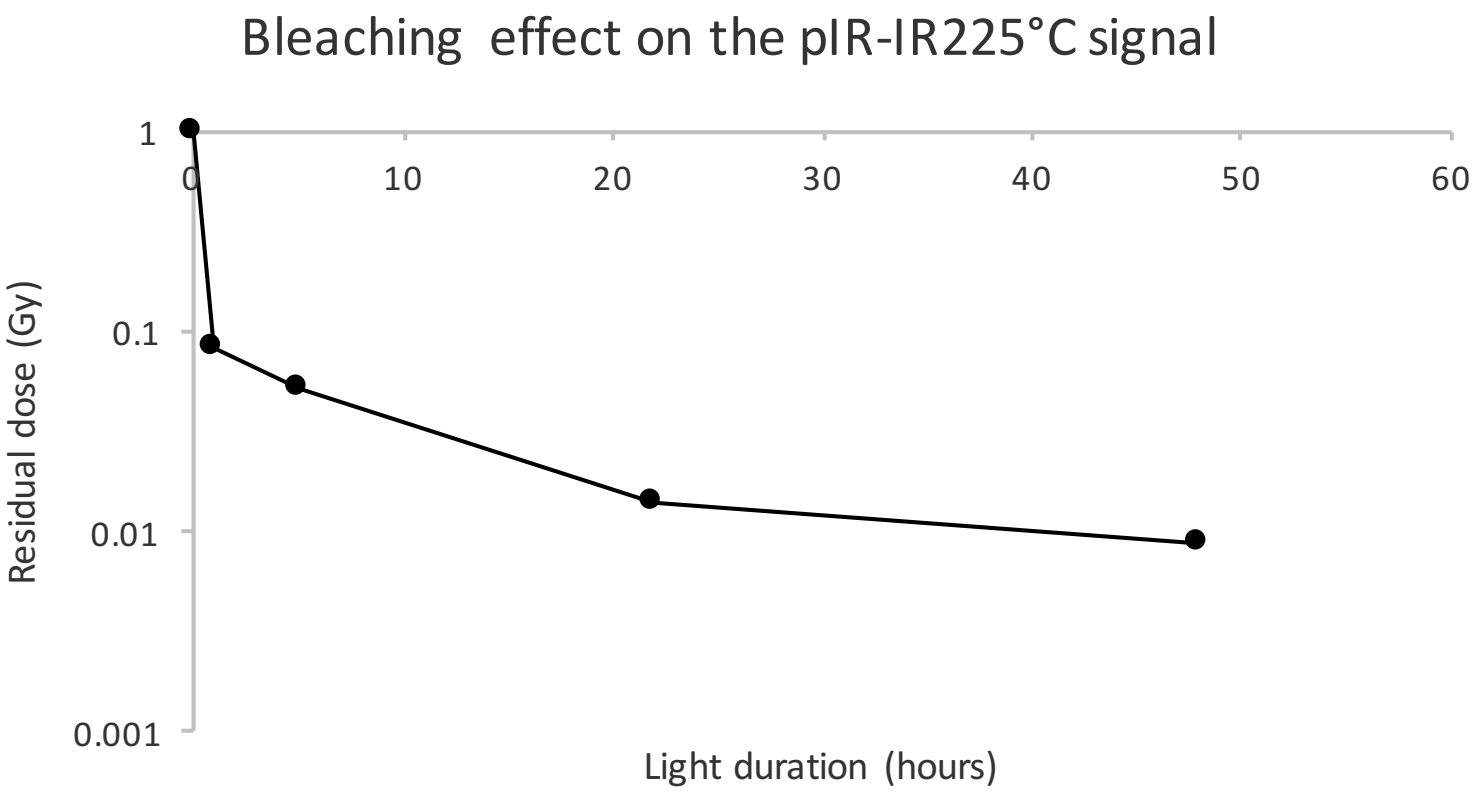
Bleaching effect on the pIR-IR225°C signal
1
0.1
0.01
0.001
0
10
20
30
40
50
60
Residual dose (Gy)
Light duration (hours)

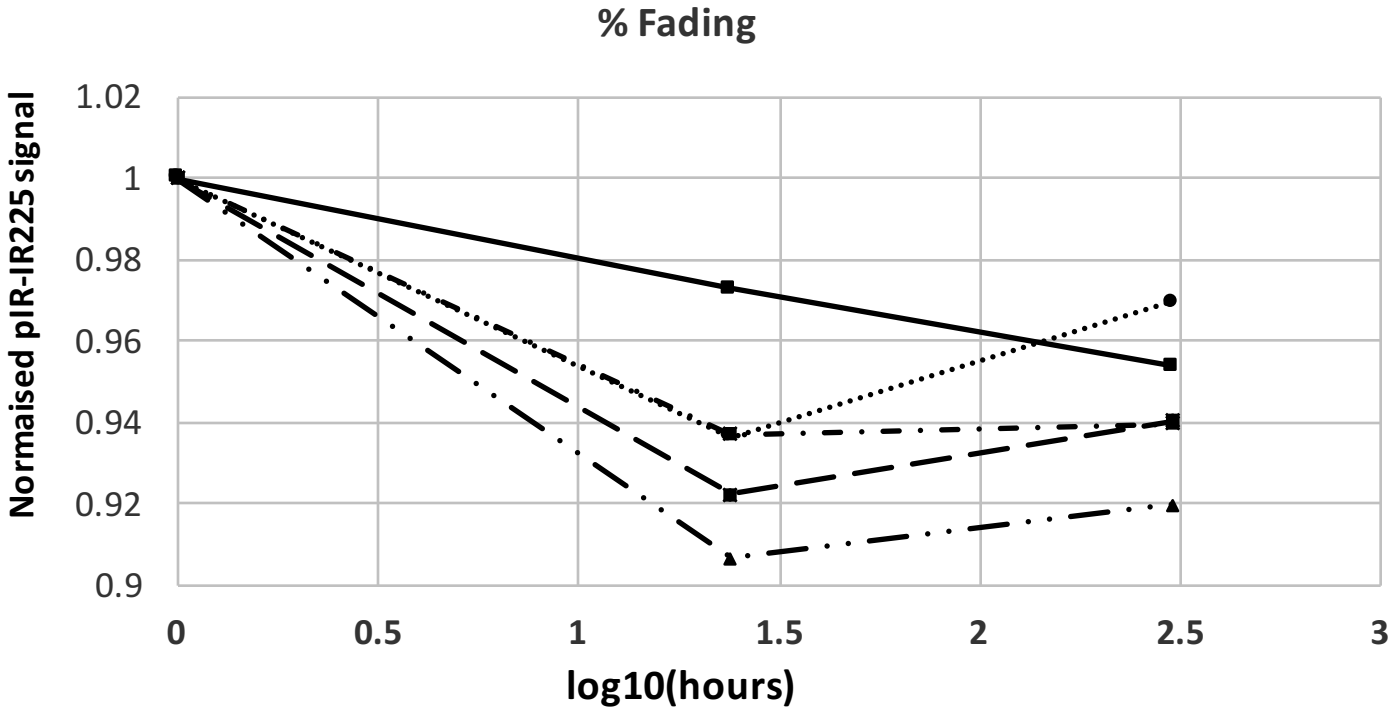
% Fading
Normaised pIR-IR225 signal
1.02
1
0.98
0.96
0.94
0.92
0.9
0
0.5
1
1.5
2
2.5
3
log10(hours)

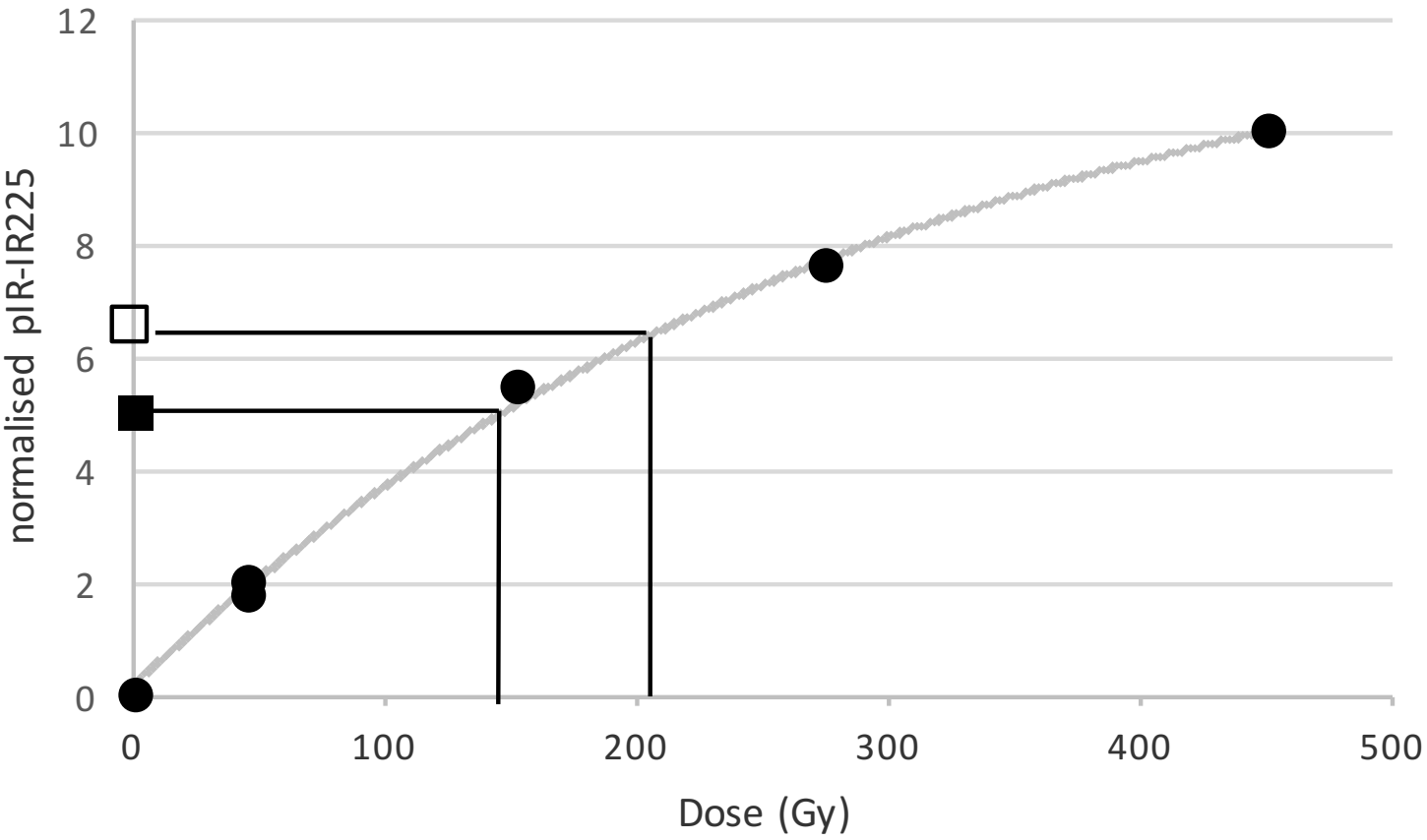
12
10
8
6
4
2
0
normalised pIR-IR225
0
100
200
300
400
500
Dose (Gy)

						QUARTZ		K-FELDSPARS	
Sample :	U (ppm)	Th (ppm)	K (%)	Ext. Beta	Ext. Gamma	Annual	±	Annual	±
S1	0.39	1.61	0.83	613	364	**1127**	**150**	**1806**	**202**
S1-2	0.45	1.42	0.81	605	270	**1025**	**120**	**1703**	**181**
S2	0.39	1.20	0.74	549	270	**969**	**77**	**1648**	**156**
S3	0.40	1.10	0.81	589	254	**993**	**80**	**1672**	**157**
S5	0.48	1.28	0.77	573	270	**993**	**85**	**1671**	**160**
L4	0.46	1.02	0.66	497	226	**873**	**73**	**1552**	**154**

Table 1

	QUARTZ				K-FELDSPARS		
					without fading corr.	with fading corr.	
Sample :	CAM-De (Gy)	OD (%)	baSAR-De (Gy)	**Age (ka)**	De (Gy)	De (Gy)	Age (ka)
S1	67.8 ± 3.2	33 ± 5	76.9 ± 4.3	**70 ± 10**	152.4 ± 3.1	206.9 ± 6.7	114 ± 11
S1-2	69.9 ± 1.2	47 ± 6	78.8 ± 4.8	**77 ± 10**	150.1 ± 4.8	207.7 ± 6.9	122 ± 12
S2	70.0 ± 2.0	38 ± 6	72.8 ± 4.9	**75 ± 8**	150.0 ± 4.6	205.8 ± 6.8	125 ± 12
S3	73.1 ± 3.5	29 ± 4	85.7 ± 6.0	**86 ± 9**	152.5 ± 5.5	211.3 ± 6.9	126 ± 12
S5	72.9 ± 2.9	35 ± 5	80.4 ± 4.5	**81 ± 8**	150.1 ± 3.3	203.6 ± 5.1	122 ± 11
L4	60.3 ± 3.9	39 ± 5	62.8 ± 3.7	**79 ± 8**	143.3 ± 4.0	199.1 ± 7.2	125 ± 9

Table 2